Journal of Casting & Materials Engineering Vol. 5 No. 4 (2021) 66–70
https://doi.org/10.7494/jcme.2021.5.4.66

Interaction of N with White-solidified Cast Iron Model Alloys: The Effect of Mn and Cu on the Formation of Fe and Si Nitrides

Stefan Kante, Andreas Leineweber*

TU Bergakademie Freiberg, Institute of Materials Science, Gustav-Zeuner-Str. 5, 09599 Freiberg, Germany
**e-mail: andreas.leineweber@iww.tu-freiberg.de*

© 2021 Authors. This is an open access publication, which can be used, distributed and reproduced in any medium according to the Creative Commons CC-BY 4.0 License requiring that the original work has been properly cited.

Received: 13 August 2021/Accepted: 22 September 2021/Published online: 22 October 2021/Corrected version: 13 July 2022.
This article is published with open access at AGH University of Science and Technology Journals.

Paper presented at the EUROMAT 2021: Cast Irons and Steel Making. September 13–17, 2021, Virtual Conference.

Abstract

Surface remelting and subsequent nitriding improves the surface properties of cast irons. Upon remelting, a white-solidified surface layer forms, which contains coarse Si-free eutectic cementite (θ) and Si-enriched ferrite, pearlite or martensite in the intercarbidic regions between the eutectic θ. Nitriding produces a compound layer at the surface, which is composed of ε and γ'-iron (carbo)nitrides and enhances the corrosion resistance. Nitriding of white-solidified Fe-C-Si alloys, being model materials for remelted low-alloy ferritic cast irons, has shown that Si dissolved in α-Fe notably affects the formation of ε and γ' in intercarbidic regions while Si simultaneously precipitates as amorphous nitride, X. Under process conditions only allowing for the formation of γ' in pure Fe, Si dissolved in α-Fe promotes the formation of ε over the formation γ', whereas Si-free eutectic θ transforms into nitride following the sequence θ → ε → γ'. The present work studies the nitriding of white-solidified Fe-3.5wt.%C-3wt.%-*M* alloys with additions of *M* = 1 wt.% Mn, 1 wt.% Cu or 1 wt.% Mn + 1 wt.% Cu, serving as model materials for remelted pearlitic cast irons. The presence of Mn and/or Cu causes notable deviations from the nitriding behavior known from Fe-C-Si alloys. Mn accelerates the precipitation of X in intercarbidic regions and obstructs the transformation of ε formed from Si-free θ into γ'. Cu promotes the formation of γ' in Si-rich intercarbidic regions, surpassing the ε-promoting effect of Si.

Keywords:
cast irons, surface treatment, gas nitriding, Fe nitrides, Si nitride precipitation

1. INTRODUCTION

Nitriding is frequently employed to improve the mechanical surface properties and corrosion resistance of Fe-base alloys by generating a compound layer (CL) at the material's surface, which is composed of γ'-$Fe_4(N,C)$ and ε-$Fe_3(N,C)_{1-x}$ (carbo)nitrides [1]. Grey-solidified cast irons contain coarse, non-nitridable graphite particles which lead to heterogeneities in the CL and hinder the formation of a dense CL [2]. This limits the improvement of the corrosion resistance achievable by nitriding. A strategy to overcome this problem is surface remelting to produce a white-solidified surface layer and subsequent nitriding [3, 4].

The processes occurring in the material and the CL formation during nitriding of the white-solidified surface layers are not well understood. Previous research of the current authors aimed at elucidating the nitriding behavior of surface-remelted cast irons by nitriding of white-solidified Fe-3.5wt.%C-1.5/3wt.%Si model alloys [5–8], denoted Fe-3.5C-0/1.5/3Si. The microstructure of these alloys is composed of coarse, Si-free [5] eutectic cementite (θ-Fe_3C_{1-z}), Si-enriched ferrite and pearlite (decomposed γ-Fe), and a minor volume fraction of $Fe_{23}Si_5C_4$ silicocarbide [9, 10]. The heterogeneous distribution of Si in the microstructure is retained during nitriding, as Si diffusion is only very short-range at typical nitriding temperatures of < 580°C.

Upon nitriding at process conditions only allowing for the formation of γ' from pure Fe, denoted **γ' conditions**, it was shown that Si-free eutectic θ exhibits the nitriding behavior of Fe-C alloys [6]. Under γ' conditions, θ first transforms into ε, which is explained by a structural relation of ε and θ as well as a higher C-solubility in ε than in γ' [7]. Afterwards, this ε transforms into γ' as expected for γ' conditions due to the release of ε-stabilizing C to the nitriding atmosphere. The nitriding behavior of Si-rich regions is complicated. Si, being regarded as a "weak nitride former" [11], very slowly precipitates as nanosized, amorphous nitride, here denoted X, in α-Fe. X is typically believed to have the elemental composition Si_3N_4 [12–14]. The present authors, however, have provided evidence that X has a composition $(Si_3N_4)_{1-x}(Fe_3N_2)_x$ with $x < 0.43$ [5]. The slow formation of X in α-Fe affects the type and the growth of the Fe nitride forming from α-Fe, which continuously depletes in Si due to the precipitation of X. Residual Si dissolved in α-Fe promotes the formation of ε over the formation

of γ' under γ' conditions. The growth of ε into α-Fe(Si) runs in a eutectoid fashion by the reaction α-Fe(Si) → ε+X [5]. The ε-promoting effect of Si was ascribed to a higher Si solubility in ε than in γ' [15], and is enhanced by C supply from the substrate to the CL during nitriding.

The nitriding behavior of surface-remelted ferritic low-alloy cast irons (GJS-400-15, GJV-300), containing only negligible additions of alloying elements other than C and Si, compares with the nitriding behavior of the Fe-C-Si model alloys studied by the present authors: Si-free θ transforms into nitride according to the above transformation sequence θ → ε → γ' and Si-stabilized ε forms from α-Fe in Si-rich ferrite/pearlite under γ' conditions [4]. In contrast, Si-rich ferrite/pearlite was found to contain mainly γ' (instead of Si-stabilized ε) in remelted and nitrided pearlitic cast irons (GJS-600-3, GJL-250$_{mod}$ [3]), containing additions of both about (0.3–0.6) wt.% Mn and 0.7 wt.% Cu [4]. The reason for the different nitriding behavior of remelted ferritic and pearlitic cast irons is uncertain. For instance, the acceleration of the otherwise slow precipitation of X due to the presence of Mn and/or Cu might lead to a faster depletion of α-Fe in Si, reducing the ε-promoting effect of Si. Different solubilities of Mn and/or Cu in ε and γ' might affect the stability range of ε and γ', and, thus, the type of Fe nitride forming under given process conditions.

In view of the different nitriding behavior of remelted ferritic and pearlitic cast irons containing different levels of Mn and Cu, the present work studies the nitriding behavior of white-solidified Fe-3.5wt.%C-3wt.%Si alloys with additions of Cu, Mn and Mn+Cu. By this, first insight into the individual and combined effect of Cu and Mn on the nitriding behavior of remelted cast irons is gained. The results are compared with findings previously reported by the present authors for white-solidified and nitrided Fe-3.5C-0/1.5/3Si model alloys [5–8].

2. EXPERIMENTAL

Fe-3.5C-3Si-*M* (*M* = 1Cu, 1Mn, 1Mn-1Cu) alloys – all numbers represent nominal element contents in wt.% – were produced from pure elements supplied by Alpha Aesar (Fe, C, Si, Mn) and VEB Spurenmetalle Freiberg (Cu) in Ar atmosphere via arc melting (Tab. 1). The alloys were cast into Cu molds measuring 30 mm in length and 5 mm in diameter. Samples with a thickness of about 1.5 mm were prepared from the castings. The samples were ground and polished prior to nitriding (final step: 1 µm diamond suspension).

Gas nitriding in a NH_3/H_2-containing gas mixture was conducted using a laboratory-scale chamber furnace. A so-called nitriding potential of r_N = 1 atm$^{-1/2}$ was applied at 540°C for 1 h, 4 h, 16 h and 48 h, i.e. γ' conditions; see Section 1. r_N is controlled by the partial pressures of NH_3 and H_2, and relates to the chemical potential of N in the nitriding atmosphere, which allows for a thermodynamics-based control of the type of Fe nitride forming at the material's surface [1]. The samples were pulled into the cold pre-chamber of the furnace to terminate the nitriding treatment; see Ref. [5] for details on the treatment.

X-ray diffraction (XRD) measurements were performed on the surface of the samples in a 2θ range of 30°–125° with a Bruker D8 ADVANCE diffractometer. The diffraction patterns were evaluated by means of the Rietveld method using the Bruker-AXS TOPAS 5 software [16] and crystal structure data in Table 2. Scanning electron microscopy (SEM) of metallographic cross-sections prepared from as-cast samples and samples nitrided for 16 h was conducted using a JEOL JSM-7800f equipped with EDAX Octane Elite EDS system (EDS: energy dispersive electron spectroscopy) and EDAX Hikari Super EBSD system (EBSD: electron backscatter diffraction). Z-sensitive backscatter electron (BSE) contrast was used for imaging, giving dark contrast to nitrides. EBSD was measured with a step-width of 50 nm. EBSD patterns were indexed based on the crystal structure data in Table 2. EBSD maps were plotted using MTEX [17].

Table 1
Nominal and measured element contents [wt.%] of the investigated Fe-3.5C-3Si-1Mn/-1Cu/1Mn-1Cu alloys

Nominal	C	Si	Mn	Cu
Fe-3.5C-3Si-1Mn	3.61	2.65	0.86	–
Fe-3.5C-3Si-1Cu	3.58	2.98	–	0.87
Fe-3.5C-3Si-1Mn-1Cu	3.47	2.66	0.96	0.99

Table 2
Crystal structure data based on Refs. [18, 19] used to evaluate data

Phase	Space group	Typical lattice parameters, Å
α-Fe	$Im\bar{3}m$	a = 2.866
γ'-$Fe_4(N, C)$	$Pm\bar{3}m$	a = 3.790
ε-$Fe_3(N, C)_{1+x}$	$P6_322$	a = 4.698, c = 4.379
θ-Fe_3C_{1-z}	*Pnma*	a = 5.090, b = 6.744, c = 4.525

3. RESULTS AND DISCUSSION

3.1. Microstructure of as-cast Fe-3.5C-3Si-*M*

The microstructures of as-cast Fe-3.5C-3Si-*M* are basically comparable to those of Fe-3.5C-0/1.5/3Si in Refs. [5–8], exhibiting coarse eutectic θ plates, decomposed primary and eutectic γ-Fe, and silicocarbide. The silicocarbide in Fe-3.5C-3Si was shown to be $Fe_{23}Si_5C_4$ [9], and might contain Mn in Fe-3.5C-3Si-1Mn/1Mn-1Cu [10]. Contrary to as-cast Fe-3.5C-0/1.5/3Si, in which γ-Fe is decomposed into ferrite and pearlite, a very large volume fraction of martensite exists in Fe-3.5C-3Si-*M*. This might be due to the retarding effects of Cu and Mn on the pearlite reaction as well as large cooling rates. The latter relate to the Cu molds used to produce Fe-3.5C-3Si-*M*, which were smaller than the molds used to produce Fe-3.5C-0/1.5/3Si in Ref. [5–8]. Pearlitic, ferritic, and martensitic microstructure regions are not distinguished and referred to as intercarbidic regions in the following, as no notable difference in the nitriding behavior was observed. EDS (Tab. 3) qualitatively shows that Si and Cu are enriched in intercarbidic regions, while eutectic θ may be regarded as Si- and Cu-free. It is believed that the measured Si and Cu contents in θ are not real [5]. Mn is enriched in eutectic θ, but is also contained in intercarbidic regions.

Table 3
Element contents [wt.%] in eutectic θ and intercarbidic regions in Fe-3.5C-3Si-1Mn/-1Cu/1Mn-1Cu estimated by EDS. Si and Cu contents in θ are likely overestimated

Alloy	Intercarbidic regions (former primary/eutectic γ-Fe)			Eutectic θ		
	Si	Mn	Cu	Si	Mn	Cu
Fe-3.5C-3Si-1Mn	4.2/6.0	0.6/0.6	–	0.1	1.1	–
Fe-3.5C-3Si-1Cu	3.5/5.3	–	1.3/0.9	0.2	–	0.2
Fe-3.5C-3Si-1Mn-1Cu	3.4/4.9	0.6/0.5	1.4/1.2	0.4	1.1	0.2

3.2. Precipitation of X in α-Fe of the diffusion zone (DZ)

A dense CL has formed at the surface of Fe-3.5C-3Si-*M* after nitriding for 16 h (Fig. 1a). The positions of former eutectic θ and intercarbidic regions, now transformed into nitride, are still visible in the CL. In the diffusion zone (DZ) underneath the CL, Fe silicocarbide is decomposed into α+X [5]. Nanosized precipitates of dark BSE contrast are visible in the intercarbidic regions (Fig. 1b). These are believed to be mainly X, however, the additional formation of Mn_3N_2 or $MnSiN_2$ [20] in Fe-3.5C-3Si-1Mn/1Mn-1Cu cannot be excluded by the current investigations. In Fe-3.5C-3Si-1Cu, precipitates of bright BSE contrast were occasionally observed, indicating the precipitation of Cu during nitriding [21]. The visible number density of X appears larger in Fe-3.5C-3Si-1Mn/1Mn-1Cu than in Fe-3.5C-3Si-1Cu, while the size of X appears smaller in Fe-3.5C-3Si-1Mn/1Mn-1Cu.

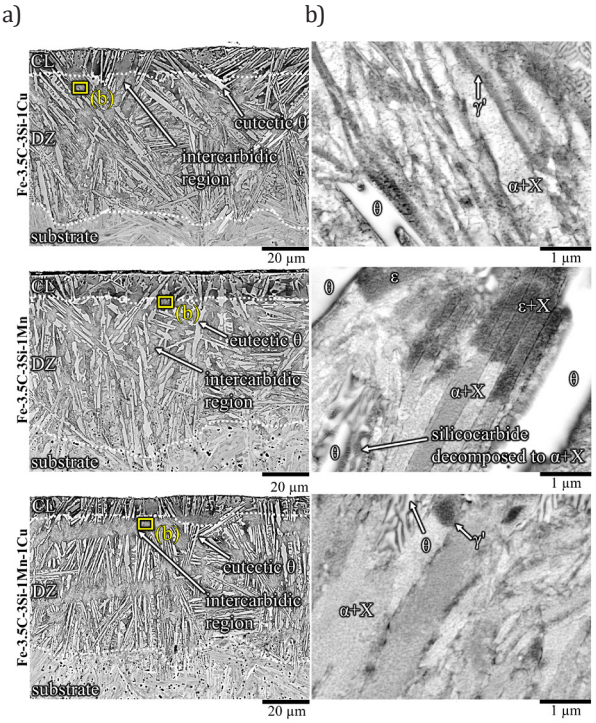

Fig. 1. SEM-BSE images of nitrided Fe-3.5C-3Si-*M* (r_N = 1 atm$^{-1/2}$, 540°C, 16 h): a) overview images showing the compound layer (CL), the diffusion zone (DZ) and the substrate; b) close-ups of the highlighted regions in (a)

Figure 2a compares the α-Fe lattice parameter, a_α, of as-cast and nitrided Fe-3.5C-3Si-*M* and Fe-3.5C-0/1.5/3Si. The precipitation kinetics and amount of X in α-Fe can be qualitatively estimated from changes in a_α during nitriding.

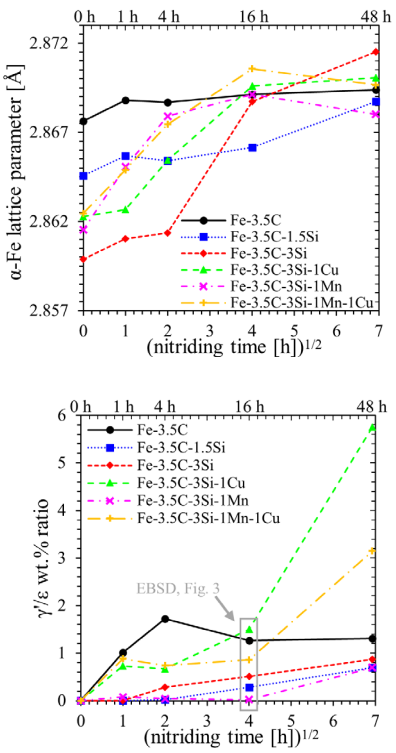

Fig. 2. Temporal evolution of the (a) α-Fe lattice parameters and (b) γ'/ε wt.% ratios in as-cast and nitrided Fe-3.5C-3Si-*M*, estimated from XRD data, compared with data of Fe-3.5C-0/1.5/3Si studied in Ref. [8]; all samples nitrided at r_N = 1 atm$^{-1/2}$ and 540°C

Generally, a_α decreases with increasing Si content in α-Fe and increases with the addition of Cu and Mn (Fig. 2a, 0 h). The depletion of α-Fe in substitutionally dissolved Si due to the precipitation of X leads to an increase in a_α with increasing nitriding time in all Si-containing alloys such that a_α in the Si-containing alloys approaches the value of a_α in nitrided Si-free Fe-3.5C. In comparison with Fe-3.5C-1.5/3Si, the increase in a_α and, thus, the precipitation of X seems to be slightly faster in Fe-3.5C-3Si-1Cu and notably faster in Fe-3.5C-3Si-1Mn/-1Mn-1Cu.

On the one hand, the precipitation of X in Fe-3.5C-3Si-*M* might be accelerated by co-precipitation of X and Cu, Mn_3N_2 or $MnSiN_2$, if the latter precipitates faster in α-Fe than X. Accelerated X formation is known from nitriding of Fe-Ti/Cr-Si alloys [22], in which X nucleates at phase boundaries of α-Fe and previously formed CrN and TiN precipitates. Moreover, $MnSiN_2$ possibly forming in addition to X may also deplete α-Fe in Si, contributing to the observed increase in a_α. On the other hand, to the authors' knowledge, crystalline $MnSiN_2$ has been observed only upon nitriding Fe-Si-Mn alloys [20, 23]

at higher temperatures or for longer times than those employed in the present study, and Mn_3N_2 was not observed upon nitriding of these Fe-Si-Mn alloys. Recently, the dissolution of Mn in amorphous X was reported [24]. Thus, the presence of Mn might also affect the thermodynamic driving force to form X. Future investigations by high-resolution techniques must clarify the nature of the precipitates in Fe-3.5C-3Si-*M* and the role of Mn in the precipitation mechanism.

3.3. Fe nitride distribution in the compound layer (CL)

Figure 2b shows the γ'/ε wt.% ratio, $r_{\gamma'/\varepsilon}$, in the CLs of Fe-3.5C-3Si-*M*, together with values of Fe-3.5C-0/1.5/3Si, after nitriding for 1–48 h under γ' conditions. After short nitriding times, both ε and γ' have formed in Fe-3.5C and Fe-3.5C-3Si-1Cu/-1Mn-1Cu, whereas almost only ε has formed in Cu-free Fe-3.5C-1.5/3Si and Fe-3.5C-3Si-1Mn. With increasing nitriding time, $r_{\gamma'/\varepsilon}$ slightly increases in Cu-free Fe-3.5C-1.5/3Si and notably increases in Fe-3.5C-3Si-1Cu/-1Mn-1Cu. γ' appears to form only after nitriding for 48 h in Fe-3.5C-3Si-1Mn.

EBSD phase maps of samples nitrided for 16 h in Figure 3 agree with the XRD results and give insight into the local distribution ε and γ' in the CLs. In microstructure regions associated with Si-free eutectic θ, the transformation sequence θ → ε → γ' (Sect. 1) is observed in Fe-3.5C-0/1.5/3Si and Fe-3.5C-3Si-1Cu. ε formed from Mn-enriched eutectic θ in Fe-3.5C-3Si-1Mn/-1Mn-1Cu (Tab. 3) seems to resist against the eventual transformation into γ', which is only occasionally visible in respective EBSD maps (Fig. 3). Thus, Mn appears to stabilize ε with respect to γ', retarding – even though not suppressing – the transformation ε → γ'.

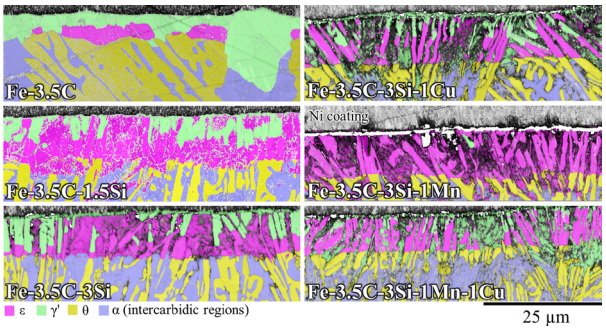

Fig. 3. EBSD phase maps of Fe-3.5C-0/1.5/3Si in Ref. [8] and Fe-3.5C-3Si-*M*, nitrided at r_N = 1 atm$^{-1/2}$ and 540°C for 16 h

Only γ' has formed in the Si-free intercarbidic regions of Fe-3.5C, whereas only ε is has formed in the Si-rich regions of Fe-3.5C-1.5/3Si due to the ε-promoting effect of Si [5–8]; see Section 1. Like in Fe-3.5C-1.5/3Si, ε has formed in the Si-rich intercarbidic regions of Fe-3.5C-3Si-1Mn. In spite of the presence of Si, however, only γ' has formed in the intercarbidic regions of Fe-3.5C-3Si-1Cu/-1Mn-1Cu. Evidently, Cu promotes the formation of γ' from Si-enriched α-Fe over the formation of ε. Even more, the γ'-promoting effect Cu surpasses the ε-promoting effect of Si.

The formation of either ε or γ' in the intercarbidic regions of the different alloys in conjunction with the differently pronounced occurrence of the transformation θ → ε → γ' explains the basic trends and differences in $r_{\gamma'/\varepsilon}$ in Figure 2b. Note that the step ε → γ' involved in θ → ε → γ' is notably time-dependent, requiring the long-range redistribution of C [6], and hardly occurs in Fe-3.5C-1.5/3Si during nitriding times shorter than 4 h at the present process conditions [8].

The Fe nitride content and distribution in the CLs in Fe-3.5C-3Si-1Cu/-1Mn-1Cu and in remelted and equally nitrided pearlitic cast irons [4] (Sect. 1) compare, whereas the Fe nitride content and distribution in Fe-3.5C-3Si-1Mn are similar to those in remelted and equally nitrided ferritic cast irons [4] and Fe-C-Si model alloys [5–8]. Based on the present findings, the difference in the Fe nitride content in remelted and nitrided (Mn+Cu)-alloyed pearlitic and Mn-/Cu-lean ferritic cast irons can be ascribed to Cu. Although the precipitation of X seems notably accelerated by Mn (Sect. 3.1), Mn does not promote the formation of γ' from α-Fe in intercarbidic regions. This means the accelerated precipitation of X in α-Fe and, thus, the accelerated depletion of α-Fe in Si does not seem to affect the type of Fe nitride forming from α-Fe. Therefore, and due to an apparently little effect of Cu on the precipitation of X, it is inferred that different Cu solubilities in ε and γ' lead to the γ'-promoting effect of Cu. Fe-Cu alloys are currently nitrided by the authors to substantiate that assumption.

4. CONCLUSIONS

The Fe nitride content and formation of Si-rich nitride, X, in Fe-3.5C-3Si-1Mn/1Cu/1Mn-1Cu alloys upon nitriding at γ' conditions (r_N = 1 atm$^{-1/2}$, 540°C) was studied by SEM, XRD and EBSD. Comparing the present results with results obtained from equally nitrided Fe-3.5C-0/1.5/3Si alloys allows for the following preliminary conclusions. Mn accelerates the formation of X in α-Fe and stabilizes ε formed from Mn-enriched θ against an eventual transformation into γ'. Cu does not seem to significantly accelerate the precipitation of X in α-Fe and promotes the formation of γ' from Si-enriched α-Fe over the formation of ε, surpassing the ε-promoting effect of Si.

Acknowledgments

The authors gratefully acknowledge the German Research Foundation for their financial support of the project LE 1403/1-2. The authors thank E. Siegismund for conducting nitriding experiments, and Dr.-Ing. T. Kreschel for analyzing the alloy compositions (both: TU Bergakademie Freiberg).

REFERENCES

[1] Mittemeijer E.J. & Somers M.A.J. (2014). Thermochemical surface engineering of steels: Improving materials performance. Elsevier.

[2] Baranowska J. (1998). Surface quality of grey cast irons in the context of nitriding and oxygen-sulphur-nitriding. *Surface and Coatings Technology*, 100–101, 271–275. Doi: https://doi.org/10.1016/S0257-8972(97)00631-2.

[3] Buchwalder A., Zenker R., Rüthrich K., Griesbach, W., Nagel K., Hartwig S. & Siedler J. (2014). Eine neue kombinierte Randschichttechnologie für hochbeanspruchte Gusseisenwerkstoffe. *HTM*, 69(3), 138–147. Doi: https://doi.org/10.3139/105.110219.

[4] Holst A., Buchwalder A. & Zenker R. (2020). Influence of gas nitriding conditions on layer structure formation on grey- and white-solidified cast irons. *La Metallurgia Italiana,* 112(1), 61–72.
[5] Kante S., Kürnsteiner, P., Gault B., Motylenko M. & Leineweber A. (2021). Eutectoid growth of nanoscale amorphous Fe-Si nitride upon nitriding. *Acta Materialia,* 209, 116774. Doi: https://doi.org/10.1016/j.actamat.2021.116774.
[6] Kante S. & Leineweber A. (2018). Nitriding of Fe-C and Fe-C-Si White Cast Iron In: H. Klümper-Westkamp, K.M. Winter (Eds.), Proceedings of the ECHT 2018, Carl Hanser Verlag, München, pp. 5–14.
[7] Kante S. & Leineweber A. (2019). Two-phase and three-phase crystallographic relationships in white-solidified and nitrided Fe-C-Si cast iron. *Acta Materialia*, 170, 240–252. Doi: https://doi.org/10.1016/j.actamat.2019.03.029.
[8] Kante S., Motylenko M. & Leineweber A. (2021). Nitriding of White-Solidified Fe-C-Si Alloys: Diffusion Path Concept Applied to Inhomogeneous Microstructures. *Advanced Engineering Materials*, 2100833. Doi: https://doi.org/10.1002/adem.202100833.
[9] Kante S. & Leineweber A. (2020). The iron silicocarbide in cast irons revisited. *Journal of Alloys and Compounds,* 815, 152468. Doi: https://doi.org/10.1016/j.jallcom.2019.152468.
[10] Spinat P., Brouty C., Whuler A. & Herpin P. (1975). Etude structurale de la phase 'Mn_6Si_2C'. *Acta Crystallographica Section B: Structural Science, Crystal Engineering and Materials*, 31, 541–547. Doi: https://doi.org/10.1107/S0567740875003196.
[11] Steiner T. & Mittemeijer E.J. (2016). Alloying Element Nitride Development in Ferritic Fe-Based Materials Upon Nitriding: A Review. *Journal of Materials Engineering and Performance*, 25, 2091–2102. Doi: https://doi.org/10.1007/s11665-016-2048-x.
[12] Mittemeijer E.J., Biglari M.H., Böttger A.J., Van der Pers N.M., Sloof W.G. & Tichelaar F.D. (1999). Amorphous precipitates in a crystalline matrix: Precipitation of amorphous Si_3N_4 in α-Fe. *Scripta Materialia*, 41(6), 625–630. Doi: https://doi.org/10.1016/S1359-6462(99)00143-8.
[13] Van Landeghem H.P., Gouné M., Bordère S., Danoix F. & Redjaïmia A. (2015). Competitive precipitation of amorphous and crystalline silicon nitride in ferrite: interaction between structure, morphology, and stress relaxation. *Acta Materialia*, 93, 218–234. Doi: https://doi.org/10.1016/j.actamat.2015.04.032.
[14] Meka S.R., Jung K.S., Bischoff E. & Mittemeijer E.J. (2012). Unusual Precipitation of Amorphous Silicon Nitride Upon Nitriding Fe-2at.%Si Alloy. *Philosophical Magazine*, 92 (11), 1435–1455. Doi: https://doi.org/10.1080/14786435.2011.648226.
[15] Meka S.R. & Mittemeijer E.J. (2013). Abnormal Nitride Morphologies upon Nitriding Iron-Based Substrates. *JOM*, 65, 769–775. Doi: https://doi.org/10.1007/s11837-013-0603-6.
[16] Coelho A.A. (2003). Indexing of powder diffraction patterns by iterative use of singular value decomposition. *Journal of Applied Crystallography*, 36, 86–95. Doi: https://doi.org/10.1107/S0021889802019878.
[17] Bachmann F., Hielscher R. & Schaeben H. (2011). Grain detection from 2d and 3d EBSD data – Specification of the MTEX algorithm. *Ultramicroscopy*, 111(12), 1720–1733. Doi: https://doi.org/10.1016/j.ultramic.2011.08.002.
[18] Wriedt H.A., Gokcen N.A. & Nafziger R.H. (1987). The Fe-N (Iron-Nitrogen) system. *Bulletin of Alloy Phase Diagrams*, 8, 355–377. Doi: https://doi.org/10.1007/BF02869273.
[19] Leineweber A., Shang S.L. & Liu Z.K. (2015). C-vacancy concentration in cementite, Fe_3C_{1-z}, in equilibrium with α-Fe[C] and γ-Fe[C]. *Acta Materialia*, 86, 374–384. Doi: https://doi.org/10.1016/j.actamat.2014.11.046.
[20] Jonsson-Holmqvist B., Grieveson P. & Jack K.H. (1973). The nitride hardening of ferritic iron-manganese and iron-manganese-silicon alloys. *Scandinavian Journal of Metallurgy*, 2(1), 35–38.
[21] Takahashi J., Kawakami K. & Kawasaki K. (2019). Study on complex precipitation kinetics in Cr- and Cu-added nitriding steels by atom probe tomography. *Acta Materialia,* 169, 88–98. Doi: https://doi.org/10.1016/j.actamat.2019.03.002.
[22] Schwarz B., Rossi P.J., Straßberger L., Jörg F., Meka S.R., Bischoff E., Schacherl R.E. & Mittemeijer E.J. (2014). Coherency strain and precipitation kinetics: crystalline and amorphous nitride formation in ternary Fe-Ti/Cr/V-Si alloys. *Philosophical Magazine*, 94, 3098–3119. Doi: https://doi.org/10.1080/14786435.2014.952258.
[23] Roberts W., Grieveson P. & Jack K.H. (1972). Precipitation of Silicon Nitrides and Manganese-silicon Nitrides in Steel. *The Journal of the Iron and Steel Institute*, 210, 931–937.
[24] Klemm-Toole J., Burnett M., Clarke A.J., Speer J.G. & Findley K.O. (2021). Influences of Vanadium and Silicon on Case Hardness and Residual Stress of Nitrided Medium Carbon Steels. *Metallurgical and Materials Transactions A*, 52, 462–482. Doi: https://doi.org/10.1007/s11661-020-06063-x.